Submillimeter Array Technical Memorandum

Number: 52
Date: October 25, 1991
From: P. Cheimets
Subject: Azimuth and Elevation Servo Performance Predictions

MEMORANDUM

To: W. Bruckman
From: P. Cheimets
Date: July 15, 1991
File: /usr2/people/cheimets/wp/pnc91_03
Subject: Azimuth and Elevation Servo Performance Predictions
Reference:
Copies: R.B.Dias
G.U.Nystrom
E.Silverberg

1. ABSTRACT:

The pointing response of the SMA antenna azimuth and elevation axes was simulated using measured and calculated disturbances. It was found that viable control systems are achievable for both axes. The elevation drive requires careful design to deal with the effects of the torque imbalance. Reduction of the imbalance permits an increase in control authority and a decrease in pointing error from a given disturbance.

The predicted errors due to the tracking system alone are shown below for 14.1 m/s wind, friction and motor induced torque ripple. For this table, bandwidth indicates the highest frequency at which the controller produces unity gain between the position command and the position output. NOTE: Table entries marked "NOMINAL" imply a value too small to affect the root sum square error estimate of the total error (generally 1/10th of the largest contributors). The results are based on structural springs that have been calculated to produce 15 Hz natural frequencies at certain inertias and elevation angles. These values have been used throughout.

TABLE 1 Synopsis of Results

MODEL	BANDWIDTH	ERROR		
		WIND	FRICTION	RIPPLE
	Hz		ARCSEC-RMS	
Azimuth	18	0.3	0.2-3.6	0.08
Elevation -CF/CF-30°	4	0.73	NOMINAL	0.3
Elevation -Steel/CF-30°	2.5	1.10	NOMINAL	0.63
Elevation -CF/CF-Zenith	5	0.96	NOMINAL	N/A
Elevation -CF/CF-Red. Imbal.	18	0.60	NOMINAL	0.2

2. *INTRODUCTION:*

SAO has developed a pointing control system simulation as part of the overall effort to produce a specification for the Submillimeter Array (SMA) antenna construction. The array consists of 6 or more telescopes/antennas tentatively slated for construction on Mauna Kea in Hawaii. The antennas will operate in the open under ambient condition, at anytime of the day. In operation the antennas are required to point to an accuracy of 1 arcsec when repositioned less than 10 deg and to track that sky position against disturbances and sidereal motion to within 1.5 arcseconds. This requirement holds in winds up to 14.1 m/s.

In an effort to accomplish this task we have developed two representative, but low order system models that simulate the tracking performance of the azimuth and elevation axes. These are linear models permitting rapid assessment of various compensation techniques in light of the known disturbances. Though the true system is clearly non-linear, we predicted the performance of the system using a linear model, limiting the scope of the survey before we went onto more complex nonlinear models. In general, the effects of the nonlinearities were gaged using the linear models, though some nonlinear simulations were performed.

An overall mechanical design was performed in tandem with a structural analysis of the antenna dish and support structure. These efforts were in considerable depth, yielding an estimate of system inertia under various conditions, minimum modal frequencies, and an overall geometric layout. This information was utilized, in greatly reduced form, to produce the five models, 1 in azimuth and 4 in elevation.

3. *THE MODELS:*

The models for this system are based on the assumption that the subsystems can be thought of as inertia/spring pairs with a natural frequency equal to the lowest mode predicted by the structural model. The plant models are mathematically rendered in the form of N/2 second order differential equations each describing a subsystem. These in turn are transformed into a set of N first order equations of the form:

$$\frac{d(x_i)}{dt} = f(x_i..x_n) \tag{1}$$

Each of these equations governs the time history of a "state" (i.e. x_i), hence this approach is called "State Space Form". Once in this form, a number of commercial analysis software tools are available to assist in the prediction of the system behavior under various conditions. In this case we used a package called MATLAB, written by MathWorks in Natick, MA.

The shortcoming of this approach is that it is inherently linear. The predicted time history of the

system depends only on the initial conditions of the states and system inputs (e.g. commanded pointing locations, model disturbance torques, etc.). Purely state dependent behavior such as friction and saturation cannot be modeled directly. In order to gauge their effects on the system, representative impulse or step functions must be applied to the model. This gives an idea of the magnitude of the system response, though it does not yield any detailed understanding of the interaction between the nonlinearity and the system dynamics; hence, it will not predict limit cycle behavior.

On the other hand the models are simple, robust and flexible. They lend themselves to rapid modification and are easy to troubleshoot. In a general way they predict system behavior and provide a surprising degree of insight into the control system design. The predicted behavior tends to be borne out by observation. Thus, this method provides a fast and easy approach to limiting the scope of inquiry to a few promising options, and a maximum control gain (i.e. Bandwidth).

Once the field has been limited to the most promising arrangements, the effects of the non-linearities can be modeled directly. This is a very specific and detailed undertaking that is not carried out in a general way. In this case we did not find anything in the non-linear modeling effort to suggest that linear estimates of the effects of the known nonlinearities were not close enough for our purposes.

3.1 Azimuth Model:

The azimuth model consists of three inertias connected by two rotary springs (see figure 1). The inertias represent the motor and drive, the yoke and cabin, and the antenna dish itself. The rotary springs model the compliance of the motor drive and the yoke/dish sub-system. The drive inertia and stiffness represent calculated values for a candidate drive, details of this calculation are presented in March 8th, 1991 report entitled *Calculations of Elevation Drive Performance.* The inertia values come from the detailed design and analysis work that was performed as part of the SAO specification effort. The second spring constant, modeled as the compliance between the motion of the yoke and the dish, was selected to set the natural frequency of the dish/spring system to 15 Hz, which is in line with the first mode that is predicted by structural analysis.

In order to mirror the actual sensor arrangement the measured quantity is the yoke and cabin position. This is the closest modeled point to the azimuth bear where the encoder will actually be mounted. This has the effect of allowing the dish to flex, open loop, in the wind. Though the compliance of the yoke/dish system is greater than in the actual system, this is the way the antenna will operate.

This modeling approach has limitations. We have assumed that the mode is torsional, and involves the whole inertia, either of these assumptions may be false. It may not be a torsional mode or it may not be a whole body mode. But these assumptions are conservative since the worst case occurs when a mode is the first natural frequency, i.e is a whole body mode, as far as predicted disturbance response is concerned. However, whatever the shape of the first mode, the controller dynamics has to be sufficiently far this mode in frequency, to keep from amplifying it.

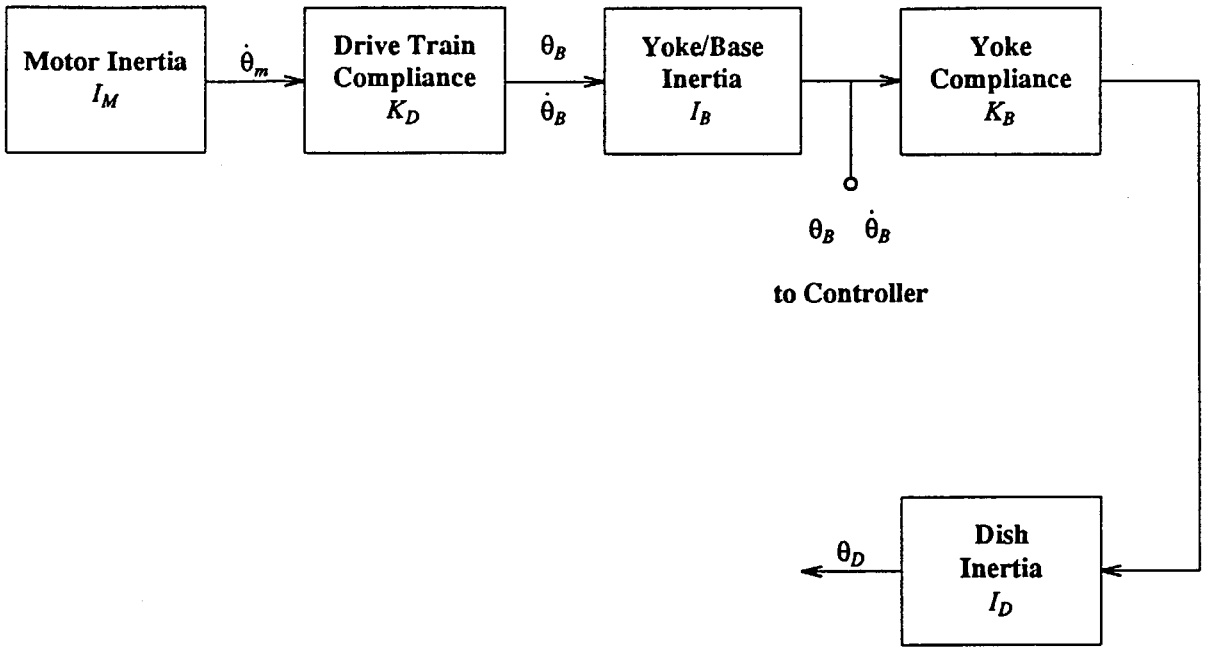

Figure 1 Block Diagram of Azimuth Model

The linear model gives us insight into this proximity.

3.1.1 Azimuth Cases: At the time this modeling work was done there were a lot of possible dish designs, all with their own inertia. This, coupled with the fact that changing the dish elevation changes the inertia about the azimuth axis, yields a large number of possible cases to run in order to get a complete picture of the azimuth servo performance. However a couple of facts mitigate against this tack. First, the various designs have a large effect on the elevation inertia but a small effect on the azimuth inertia. Second, the effect of the largest error source, the wind, on the pointing performance of this axis is highest when the dish is pointed at the horizon. Third, the effect of an azimuth error on the telescope pointing is also peaked when the dish is pointed at the horizon. Finally, though the effect of the elevation position on the azimuth inertia is small, it too is peaked when the dish is pointed at the horizon.

All these factors taken together convinced us that only one azimuth case simulation, that with the dish at its lowest elevation-- 30° above the horizon, was necessary in order to get a worst case indication of azimuth performance.

3.2 Elevation Model:

The elevation model consists of two inertias and a single spring. The inertias represent the dish and the motor (see figure 2). The spring models the entire compliance of the motor drive and dish support and is mounted between the motor and the dish. The spring is assumed to be at the 1:1 axis with a gear box and linear actuator between it and the motor. It is important to note that modeling the system in this way places the gear ratio into the system dynamics, with the first mode of the motor inertia/spring system is given by:

$$f_n=\frac{1}{2\pi}\sqrt{K_s/(I_{motor}N^2)} \qquad (2)$$

Here K_s is the spring constant of the structure, I_{motor} is the motor inertia and N is the gear ratio. This has important ramifications in this case since the gear ratio turns out to be very high. This is discussed in detail below.

The spring in this model does not exactly represent any **single** element in the actual system, and topographicly it is not positioned in the same place as most of the compliance it represents. One of the structural models predicts a 15 Hz mode that includes the dish, the yoke and the linear actuator. The spring constant of this mode was calculated using a dish inertia of 16,200 kgm^2, and the worst case effective moment arm for the linear actuator; ~0.75m coinciding with a dish position near the horizon. All later models use this same spring constant. The mode shape (see figure 3) is the dish rocking on the yoke, thus it is essentially a cantilever mode of the yoke. The mode that is modeled is simply the dish rotating about the elevation axis on a rotational spring whose compliance is selected to produce a 15 Hz natural frequency with the predicted dish inertia. The model was constructed this way for three reasons:

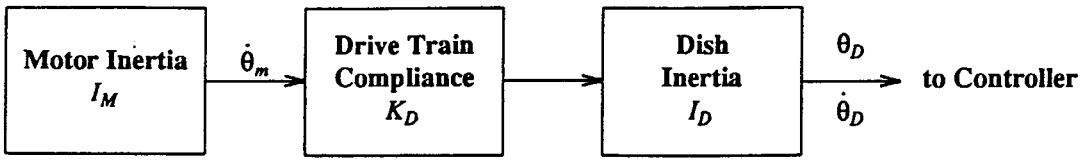

Figure 2 Block Diagram of Elevation Model

LOADCASE: 1 MODE: 1 FREQ: 18.680854
DISPLACEMENT - MAG MIN: 0.00 MAX: 1.00

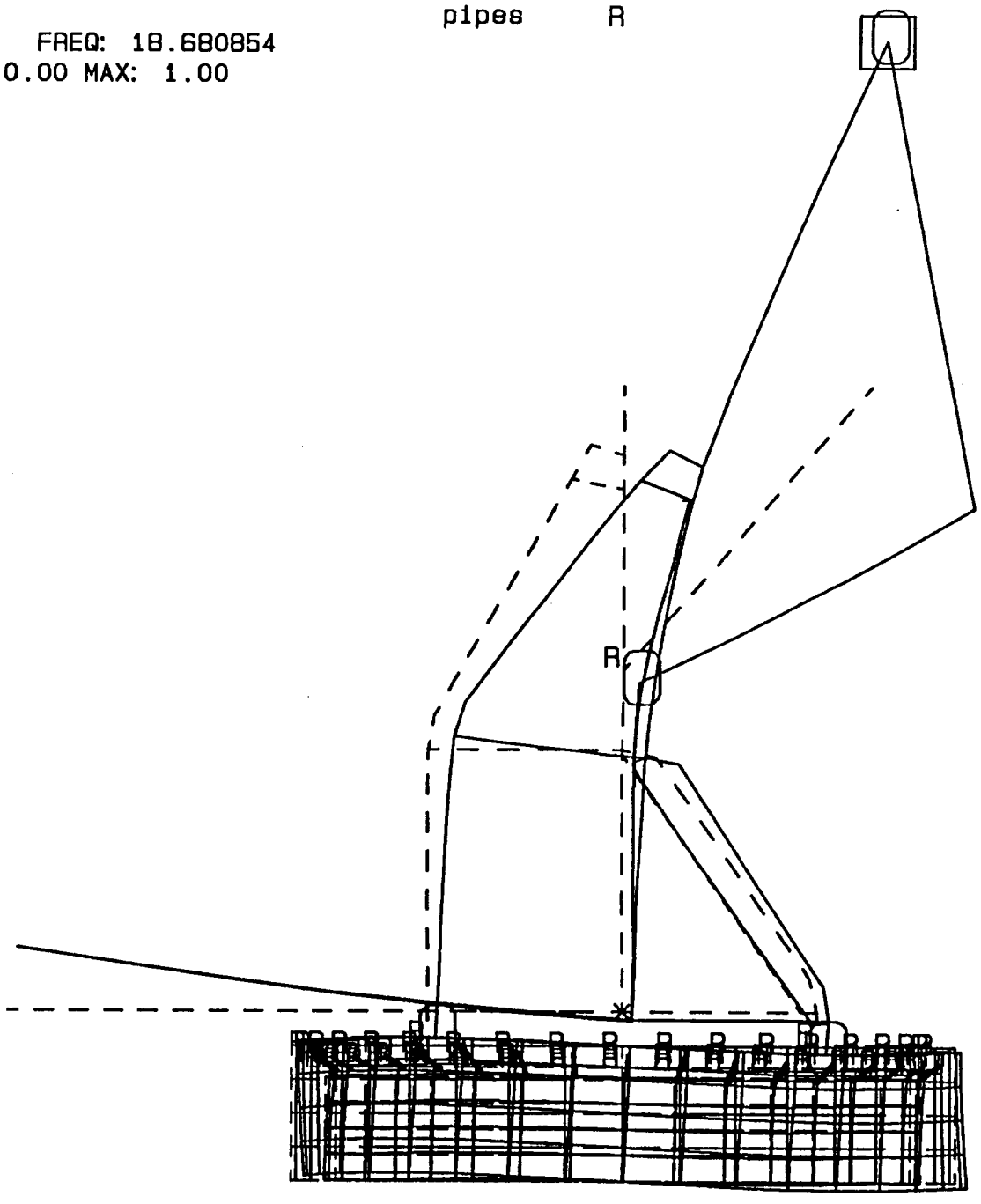

- The translational portion of the predicted mode is not important to the controls analysis;
- The yoke, in the actual system, and the spring, in the model are both free/free;
- Finally, it avoids a complex model that explicitly accounts for the yoke flexibility and the dish attachment geometry.

In the predicted mode the dish rotates and translates (moves linearly), however the linear motion does not affect the pointing directly and does not have direct bearing on the controls analysis. The linear motion does affect the pointing indirectly since the relationship between dish, the elevation axis and the linear actuator connection point changes. This fact is, however, implicit in the mode's calculated frequency.

The springs in both the controls and structural model are only excited (i.e. there is a change in force across them) when the dish is accelerated. In the structural model this results from the fact that the dish is not rotating about its center of mass, causing a reaction torque at the elevation axis when the dish is torqued. In the controls model this is represented by the spring being placed between the motor and the dish, zero torque motion of the motor would not affect the spring, while accelerating the dish would. This arrangement differs from a spring that is connected from the dish to ground that would produce a change in force across it simply by moving the dish.

It was decided that the selected model would adequately represent the true dynamics without carrying the overhead of a complex model. The extra modeling effort would only give us insight into the translational portion of the mode that is, as stated above, not the interest of the controls model.

All of the caveats related to linearity of the model apply here, though the largest nonlinearity in this axis, torque ripple, is fairly easy to model linearly.

3.2.1 Elevation Cases: Unlike in the azimuth axis model, the various dish designs represent large changes in the elevation inertia. Furthermore, though the elevation inertia is invariant with elevation position, the gear ratio between the dish and the motor does change. This is the result of a linear drive whose effective moment arm is a function of the geometry of the system, changing as the dish is rotated. The dynamics are different at different elevation angles, and without a simulation its hard to tell which angle is the worst case. Finally, all the designs use an imbalanced dish, a fact that indirectly affects the dynamics. For completeness reducing the imbalance was also explored.

All this taken together we report 4 cases here: two representing the extremes of both inertia and imbalance, run at 30°, a case run at zenith using the lowest inertia design, and finally a case run with a reduce imbalance at 30° above the horizon. The reduced imbalance case uses the design option with the lowest inertia, with half the imbalance removed by an assumed counterweight, and the inertia adjusted accordingly.

3.3 Disturbance Model:

In the prediction of any control system performance some estimate of the likely disturbances is required. In this case four primary sources of error were identified:

- Wind torque applied to the dish
- Bearing friction
- Torque anomalies in the drive motor
- Axis cross talk

These disturbances were assumed to be large enough to cause a problem and to be at frequencies where that they should be dealt with by the servo. It should be noted that the same disturbances were used for all modeled cases described above, permitting easy comparison of their responses. In reality there are different disturbance functions for different elevation axis positions since the relationship between the dish and the wind is a function of the relative angle between them.

3.3.1 Wind Torques: The wind torque was calculated from wind speeds measured at the proposed site using a torque model discussed in an Andrew Co. paper entitled *Wind Force on Parabolic Antennas* by H. Hirst and K.E. McKee. They related the wind induced torque to the wind speed, antenna size and offset. The equation that results for the worst case torque is given here:

$$M_t = 0.0002 * DAV^2 - 0.003 * AV^2 R \qquad (3)$$

where:

D is the dish diameter- *ft*
A is the dish area ft^2
V is the wind velocity- *mph*
R is the dish from the pivot to the dish vertex- *ft*

The wind measurements, which are discussed in several reports, (see references 1,2, and 3) are made with a pitot tube mounted on a weather vane. The pressure transducer is capable of faithfully following pressure changes faster than 20 Hz. When a preselected weather condition is encountered the computer that runs the experiment turns on and records the dynamic pressure of the wind every 0.05 seconds for 90 seconds. These data are reduced, taking into account the local air density, to determine an instantaneous wind speed (see figure 4). This time sequence of wind data can be used to determine the spectral content of the wind speed up to 10 Hz, or by applying equation (3) to each measurement, an instantaneous value for the torque can be determined (see figure 5). It should be noted that all the work done for this paper was in SI units, however it was felt that converting the above equation, with what amounted to magic number (i.e. 0.0002 and 0.003), might be a mistake that would result in errors; for this reason the wind velocities were converted to the British system, and the resulting torques converted back to SI.

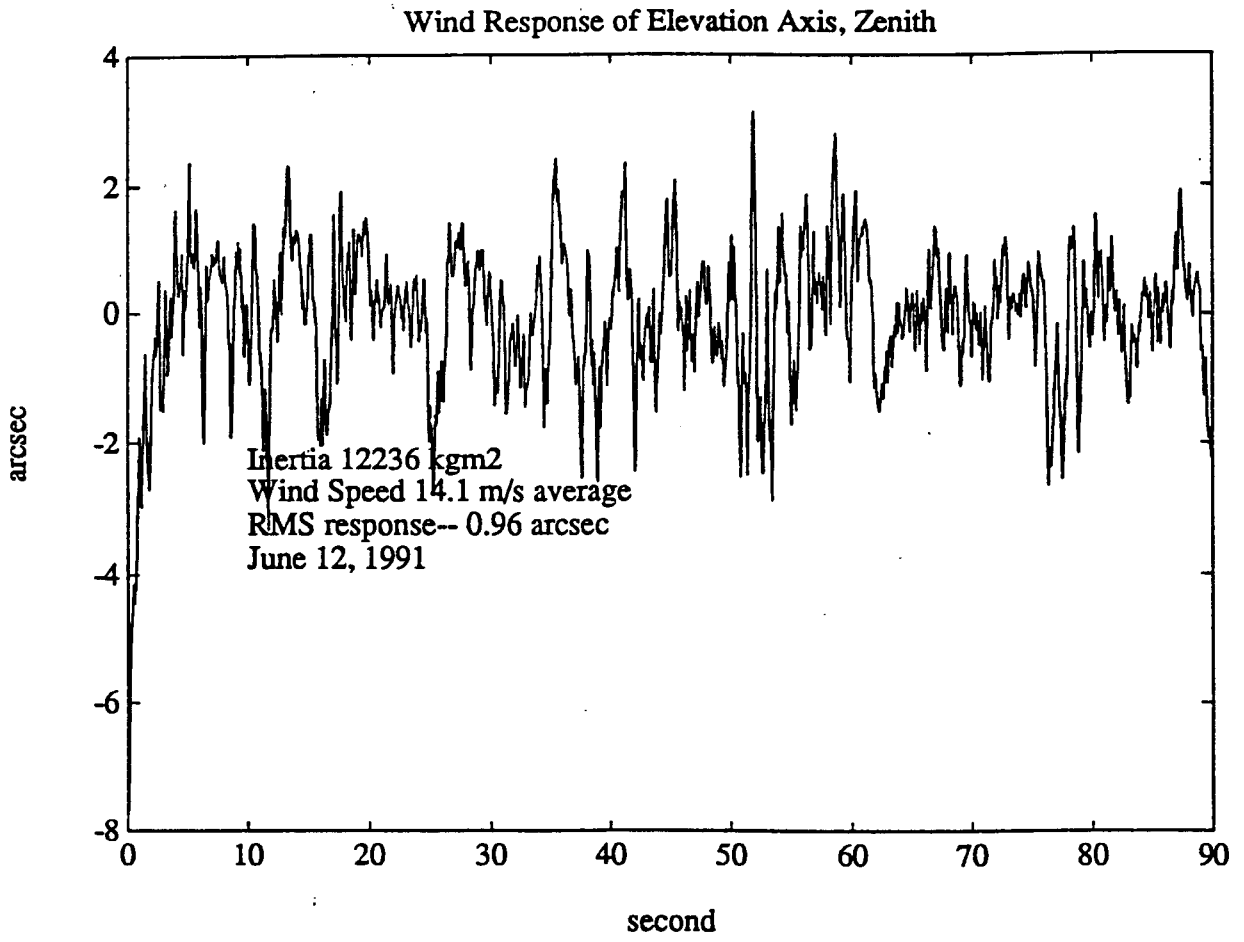

Figure 4 Representative Windspeed Data

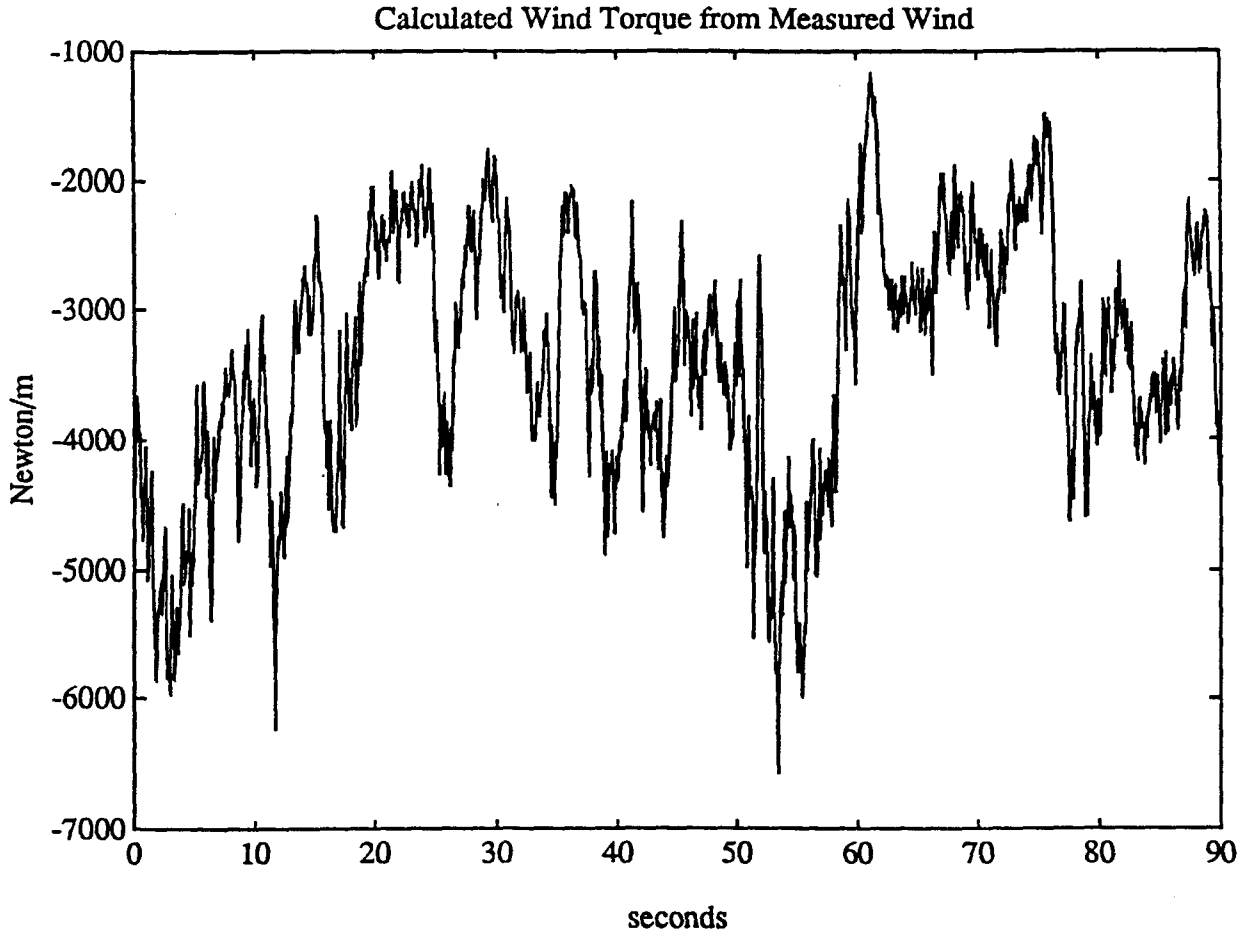

Figure 5 Calculated Torque from Measured Wind

A simulation of model behavior, when subjected to the time sequence of torque value, can then be determined with the use of the modeling software. A sample elevation model response is shown in figure (6).

3.3.2 Friction Torques: The determination of frictional torques and the resulting system response to it is an uncertain process at best. We relied on a combination of previous experience, and several reports of measured bearing friction torque (see refs 4 and 5) to produce a friction torque disturbance model.

The only axis in which the friction is a concern is azimuth, due in part to the weight of the whole system being applied to the azimuth main bearing, and the bearing's large size.

Only the varying component of friction torque is important to the controls analysis. The value of that component is generally less than 25% of the overall dynamic friction value, a number that is readily available in company literature. The other piece of information required for a complete controls analysis is the frequency content of the disturbance. This was roughly determined from the references listed above.

The data on friction torque is given spacially, this is converted to time domain by assuming a rotation rate of 15 arcsec/sec (i.e. sidereal rate). Taking the friction variations at a frequency closest to the bandwidth, the part that will affect the system the most, we determined a torque disturbance function of:

$$T_v = 0.04 * T_0 * sin(0.008 * t * \pi) \tag{4}$$

This means the important varying torque is 4% of the total dynamic friction. In estimating the system behavior when it is subject to this torque, we used the approximate form of the second order transfer function rather than perform a full computer simulation. The error is given by:

$$\delta = \frac{T_v}{I\omega^2_{BW}} \tag{5}$$

In this equation ω^2_{BW} is the closed loop bandwidth of the servo, while I is the inertia about the azimuth axis.

It should be noted that the friction calculation was performed two other ways in order to bracket the possible values. First we assumed that all of T_v, or 25% of T_0 was applied to the system, at its bandwidth frequency. Roughly, that means that T_v in equation (5) is 8 times larger. For the second calculation we assumed that the control system produced a constant speed servo, that is

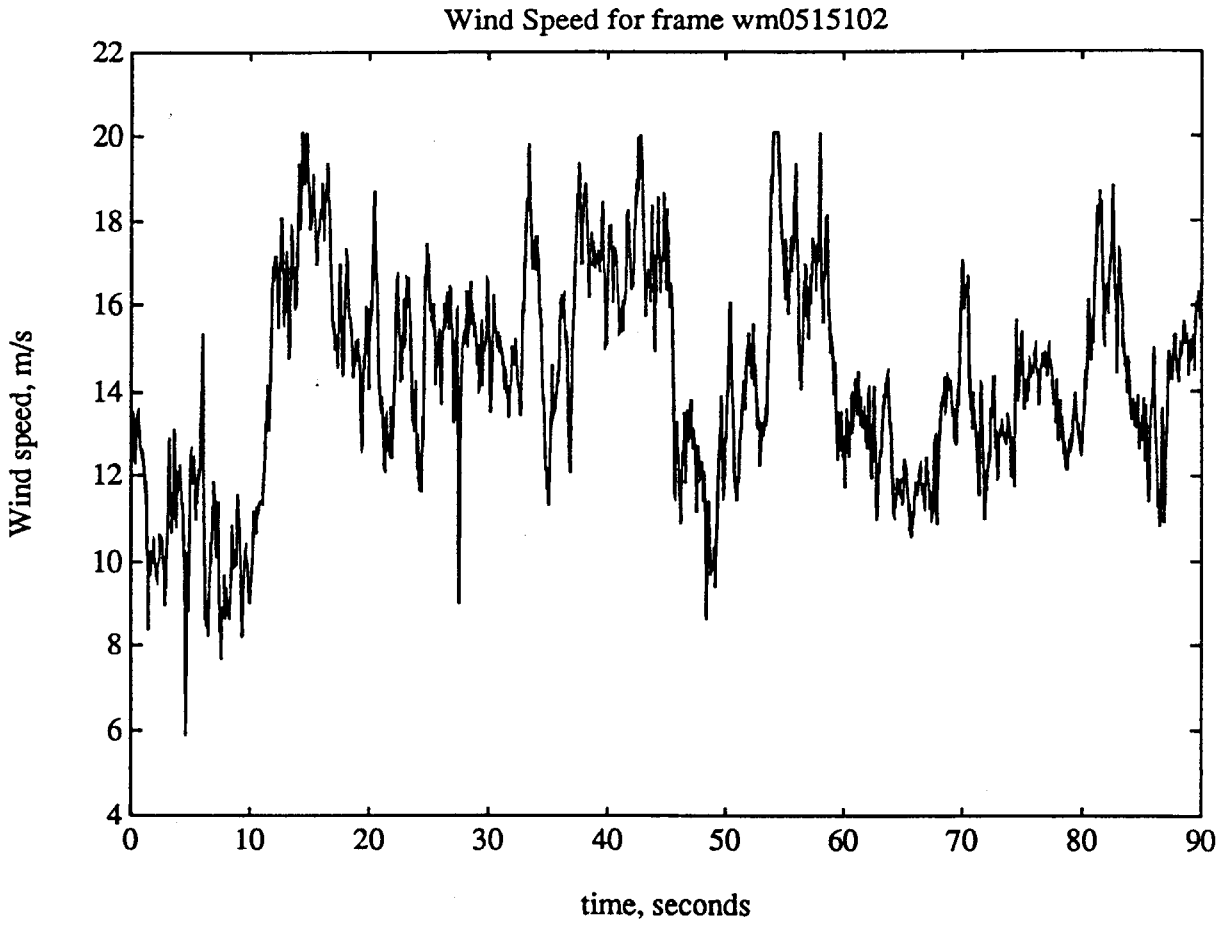

Figure 6 Simulated Response to Measured Wind

to say that the motor inertia, when multiplied by the gear ratio was much larger than the telescope inertia, this is not the case but it provides a lower limit. With this assumption the error is calculated with the following equation:

$$\delta=\frac{T_v}{K} \tag{6}$$

Where K is the drive train spring constant.

3.3.3 Motor Torque Anomalies: The most likely motor type for this application is a brushless servo. They use the latest magnetic materials in their construction and are generally designed to have the lowest inertia, an important consideration in the elevation drive system because of the large torque imbalance. When a drive system is sized for the imbalance, either by getting a very large motor or by putting a large gear ratio between the motor and the dish, the motor inertia, at the 1:1 axis, is comparable or larger than the dish inertia. This reduces the ability of the motor to overcome itself and control the dish (see below).

The primary torque anomaly from a brushless motor is *torque ripple* resulting from the electronic commutation of the stator coils. The lowest values we were able to find are between 4%-6% of the prevailing torque, varying at 6 times the rotation frequency. This results in a very large torque disturbance; see Table 2 for a list of the torque disturbances. In the table the Motor Torque is the sum of the imbalance, the wind torque and a 20% factor of safety. The ripple term, peak to peak, approaches the size of the operating wind torques, 8160 Nm at a wind speed of 21 m/s. The torque ripple varies very slowly though; during sidereal tracking its frequency is about 0.08 Hz, though this depends on the gear ratio. Estimating the effect of this disturbance is simply a matter of creating a sinusoidal time sequence with the correct amplitude, then subjecting the model to it in a linear simulation.

Table 2 Torques from Motor Ripple

Model	Torque Imbalance	Motor Torque	Torque Ripple
		Nm	
Elevation -CF/CF-30°	33,000	50,000	3,000
Elevation -Steel/CF-30°	55,000	75,000	4,500
Elevation -CF/CF-Red. Imbal.	16,600	30,000	1,800

3.3.4 Axis Cross Talk: Since the elevation dish is not dynamically balanced around the azimuth axis, it is possible to induce inertial torques around the elevation axis with motions in the azimuth axis. In practice this coupling is very small. The effect was estimated but not modeled.

3.4 System Errors

The only sources of error that were examined are motor saturation and encoder resolution. This was done by converting the linear models to a nonlinear model and re-simulating, this time with the effect of resolution and motor saturation in the model. The same software package was used, but a different integrator. Neither of these effects were a problem, for specifics see the results section below.

4. Control System Model:

4.1 Control Law Design:

The control requirements and the plant topography make it desirable to use classic controls techniques to determine the control law. For the most part there are no hidden states that are useful in controlling this antenna, so we have avoided modeling an estimator or trying a full state feedback design, methods that are from "modern control theory". The central portion of the law is a proportional plus derivative plus integral (PID) controller. Simply stated the compensation signal is constructed by taking the difference between the commanded and actual position, sometimes called the error signal (see figure 7), determining its derivative and integral with respect to time, scaling each of these three signals separately and combining them. The proportional signal (KP) acts like a spring, forcing the system to the commanded position at a torque level that is proportional to the error. The derivative signal (KD) produces damping, removing overshoot from the system. Finally, the integral signal (KI) eliminates "hang off", the tendency for a system to stop at a point other than the desired value because of friction, etc. This will happen if the friction torque equals the proportional feedback signal and their is little momentum left in the antenna. The integral signal will get larger, the longer the error remains, until the "hang up" is overcome. This is very useful in real systems, but the addition of an integrator tends to slow the response down and promote limit cycles when there are large nonlinearities.

Since the primary goal of the servo system is to produce an antenna that tracks well we added velocity feed forward (KVF). This creates an error signal based on the difference between the desired tracking rate and the measure antenna velocity. This value is fed directly to the torquer, compensating errors in rate. This is intended to reduce the tracking errors and is one of the primary methods used in the MMT tracking loop to achieve the high tracking performance that they report. There are other approaches to achieve this end, namely adding second integral feedback, but they tend to adversely affect the system dynamics.

In the actual implementation of the controller the velocity terms of the servo are likely to be imbedded in the motor along with any tachometer feedback that may be required. This would make them the responsibility of the antenna contractor. The position and integral portions of the loop will be in the pointing controller and therefore be part of SAO responsibility. The two parts of the system must work together and their final operation should be as it is simulated here.

Though the control law is very much classical, the mathematical implementation is not. Classical controls implementation assumes that a true integrator or differentiator is impossible to achieve. However, in a software controller these are straightforward. Since it is assumed that the loop will be closed in software, the control utilizes pure integrators and differentiators.

4.1.1 Azimuth Specifics: The position error signal in the azimuth loop model, as in the actual system, is the difference between the yoke position and the command position. To the extent that the dish follows the yoke, the dish position is controlled. The dish/spring system can be viewed as an uncontrolled mass/spring trading energy with the controlled system below. Furthermore, to the extent that torques are applied to the dish and into the system (as with wind), the dish will have a persistent offset from the position controlled within the loop. This behavior is seen in the linear model, and is representative of what will happen in reality to the extent that the dish compliance models the actual yoke compliance. Because of this loop layout the tracking performance of the azimuth loop is the difference between the command signal and the yoke position, not the dish position, for which there is no direct information.

4.1.2 Elevation Specifics: There are not any real anomalies in the elevation control law, the actual dish axis position is the controlled state.

4.2 Setting Feedback Parameters:

Selecting the feedback parameters for each of these control systems starts by calculating values for the proportional and derivative feedback constants based on two assumptions:

- The desired dynamics can be selected;
- The final controlled system can be described by a second order system.

Neither of these assumptions is terribly good but they do provide a **starting point** from which adjustments can be made. The limitation of the first assumption is that the final dynamics can only fall within a certain range, generally having a lowest eigenvalue such that $\omega_{EV} < \omega_{M1}$, where ω_{M1} is the first mode frequency of the open loop system. Though in practice using the second assumption and a viable plant model we has always gotten a stable system with an eigenvalue near the desired one, the amount of damping is not near the desired value. This is probably because there is energy being traded around the system that is not shed as one would predict from a simple second order model. These values are later adjusted in successive simulations until the modeled system meets the required specifications.

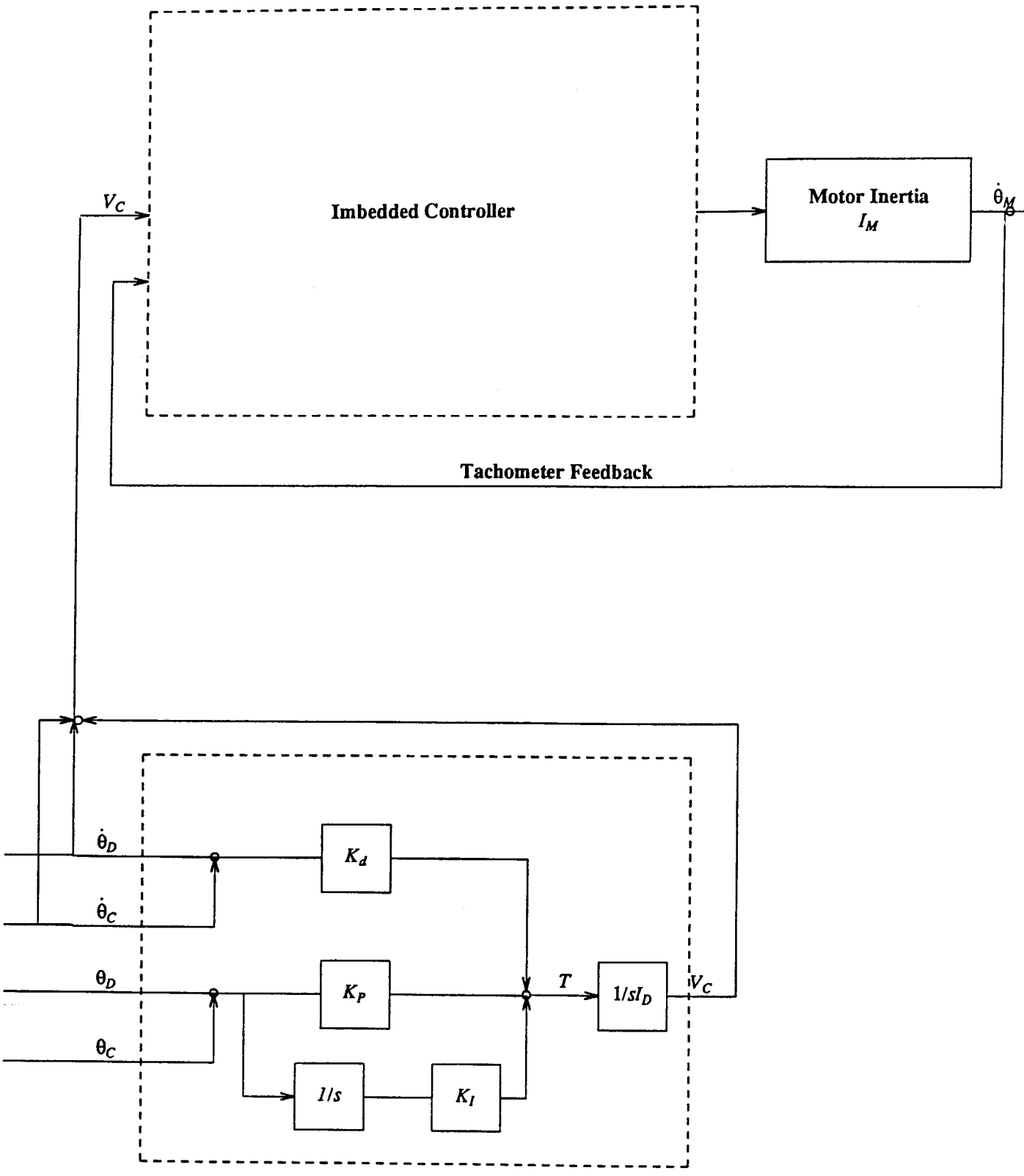

Figure 7 Block Diagram of Control System

In implementing the process of selecting the controlled system dynamics and setting the feedback parameters, we starts with equation (5). This relates the system inertia to both the bandwidth and the pointing error. The inertia comes from the model, the error from the specifications, leaving only the first eigenvalue (an indicator of the resulting system bandwidth) as a free parameter. With this selected, we use two forms of the standard second order differential equation describing dynamic motion in order to select the correct feedback values. The first equation uses system parameter explicitly:

$$I\ddot{\theta}+B\dot{\theta}+K\theta=T_c \tag{7}$$

Here B represents the ratio of torque to relative motion, and K is the displacement related torque constant, a sum of spring constants and proportional feedback. The second equation is the general form in terms of the resulting dynamics:

$$\ddot{\theta}+2\zeta\omega_N\dot{\theta}+\omega_N^2\theta=\frac{T_c}{I} \tag{8}$$

Here ζ is the damping ratio while ω_N is the natural frequency, i.e. the desired eigenvalue.

By matching up the coefficients of the two equations and determining the correct values of B and K such that you can achieve the desired values of ω_N and ζ, we are able to get a starting point for the desired compensation. It should be noted that in this simplistic approach ζ is always selected to make the servo "critically" damp, meaning that there is a compromise between speed of response and oscillation. In a general second order closed loop servo ζ is a measure of how quickly the system looses or "damps away" energy. ω_N is the equivalent of the natural frequency in naturally oscillating system, but here it is generally interpreted to be the "bandwidth" of the servo, meaning it sets the upper frequency limit on the unit response of the servo to a command input, above this the servo begins to roll off, following faster command changes with reduced fidelity. After simulating the system it became clear that ζ is at least as important as ω_N is in determining wind response.

The constants for the velocity feedforward and the integral feedback where determined within the model by trial and error. In all cases it was found that we got adequate tracking with unity feedforward, and the integral feedback constant, in general, being equal to the proportional feedback. Integral feedback is required to reduce simulated wind-induced pointing offset.

There are other, more precise approaches to the selection of feedback parameters. Modern control theory has come up with several automated optimization techniques, primarily methods to produce full and reduced state feedback. We would suggest that from some points of view this would be a good approach. We avoided them however because we did not wish to tie ourselves to a control law that need information about all the states, including motor position, etc., states that had no direct bearing on the pointed axis. Furthermore, one losses sight of the physical significance of the model parameters in a large model, and by adding automated parameter selection, all insight into the real hardware system would be lost. These techniques are there, and we would have used them if we were unable to achieve a reasonable solution otherwise.

4.2.1 Parameters for Different Elevation Cases: For the most part the same compensation was used for all the different elevation models, however in the reduced imbalance case the parameters were adjusted. This was done to examine the possible improvement.

4.3 Motor Selection:

4.3.1 Azimuth: Selecting a motor for the azimuth drive is straightforward. The motor must be able to drive the dish in a 20 m/s wind to a stow position. This required torque is small compared to the inertia. Since we felt that we would like to avoid long gear trains, thus avoiding the problems that are inherent in systems that use them (such as backlash, large reflected torques, friction, etc), we selected a drive that had a single gear pass between the motor and the bull gear (likely one of the races of the main bearing) with a selected gear ratio around 15:1. After simulating the response in this axis it was clear that if backlash were not a problem (i.e. there was a good torque bias arrangement) much larger gear ratios were possible without encountering problem related to reflected inertia. Thus it would be possible to use a much smaller motor, though the power requirements remain constant. The matter was not pursued further and the quoted results are for the larger motor.

4.3.2 Elevation: The elevation axis motor selection is quite difficult since the motor is required driving in a 20 m/s wind load against the torque imbalance. It must produce torques between 50,000 - 75,000 Nm at the 1:1 axis, depending on the dish structure, and the elevation angle. A high gear ratio is needed to achieve these high torques. The difficulty that this produces became clear after failing to stabilize this axis with the motor selected for the azimuth drive. The motor inertia, reflected through the gear train to the 1:1 axis was enormous, much larger than the dish inertia. In essence the servo motor, though forced by the control law to respond to the dish position, can not overcome its own inertia; in extreme cases the motor inertia/spring system simply oscillates.

Upon a careful examination of the system it became clear that the important parameter in dealing with this problem is the motor position term in the equation that describes the motor dynamics at the 1:1 axis. If we look at equation (8) we can see that this is the natural frequency of the motor/spring system. By keeping the frequency at least as high as the structural first mode, we are able to keep it from dominating the system response. This gave us a frequency requirement that was combined with the needed torque to produce a single inequality relating the motor inertia to its continuous torque rating. This inequality, shown below, was used as a motor specification:

$$T_{motor}^2 \geq \frac{I_{motor}}{K}\left\{\frac{2\pi f_n T_D}{A}\right\}^2 \qquad (9)$$

In this inequality f_n is the desired motor/spring natural frequency, K is the spring compliance in the elevation loop, T_D is the total required torque at the dish, and A is the linear drive moment arm. Using a torque requirement of 50,000 Nm, an f_n of 18 Hz to reduce its affect of the final

system dynamics, and a K of $256e^6$ Nm/rad, results in a derived motor specification of:

$$T^2_{motor} \geq I_{motor} * 1.04e^5 \quad (10)$$

Below is a table showing the motors that were reviewed and how they rated in the inequality.

Table 3 Motor Selection

Model #	Torque Rating	Inertia	Inequality	Accept?
	Nm	kgm^2		
Brushless Motors				
Compumotor KH710	7.3	$480e^{-6}$	53>50	Yes
Moog 303-030A	1.7	$4.2e^{-5}$	2.8>4.4	No
304-151A	10.62	$8.2e^{-4}$	113>85.3	Yes
304-121	3.16	$1.8e^{-4}$	9.9>19.7	No
Inland 03000	2.55	$4.5e^{-4}$	6.5>46.8	No
Brush type Motors				
PMI	0.23	$9.9e^{-4}$	0.1>100	No
Porter Peerless	1.9	$1.32e^{-2}$	3.68>1400	No
MET 2HP	8.2	$9.17e^{-3}$	67>1000	No

It is clear that there is little hope of the brush type motors being effective in this application. The brushless motors, though two are acceptable, are very close themselves. It should be remembered that this selection was based on the low torque imbalance of the fully carbon fiber design.

These torque ratings are determined based on the thermal performance of the motor in still 40° C air, while bolted to a 12"X12"X1" aluminum heat sink. This performance can be increased by improving the cooling system. In the extreme the the rating can be increase by up to 200% if the motors are run filled with oil and immersed in a cooled water bath. This has the effect of improving the torque/inertia ratio and improving the resulting system dynamics.

Because of the large torque imbalance the motor torque anomalies are also quite large. This is especially a problem for the brushless motors, since they have large torque ripple. The brush type motors are less prone to the problem, having more friction but less ripple, but are unsuited for this application because of their inertias.

4.3.2.1 Reduced Imbalance: The obvious next step is to examine the effects of reducing the imbalance in the elevation system. If this can be done without radically affecting other things, it might be a good idea. A model was made of a system with an imbalance that was reduced in half, while only increasing the elevation inertia 20%. This was accomplished by adding 1630 kg at a distance of 1.2 m from the elevation axis, resulting in an added 2343 kgm^2 of inertia about the axis. The gear ratio drop and the reflected inertia of the motor went down to a quarter. The

results are shown in the next section.

5. RESULTS:

5.1 Azimuth Results:

5.1.1 Linear Results: The azimuth values that were used in the model are those for the dish set at 30° above the horizon. This yields the largest wind torque, inertia, and effective error on the sky, thus it's the worst case. Only one case was run since the various dish construction methods do not have a large effect on the azimuth inertia. The model parameters and results are given in table 4.

TABLE 4 Azimuth Results

PARAMETERS	
Total Inertia	44,000 kgm^2
Dish Inertia	7400 kgm^2
Motor Inertia	0.16 kgm^2
Gear Ratio	15:1
Bearing Diameter	2.2 m
RESPONSE	
Bandwidth Frequency	18 Hz
Step Response-- Overshoot	20%
Step Response-- Settling Time	<1 sec
Tracking Error in 14 m/s Wind	0.3 arcsec RMS
Tracking Error from Friction	0.06-1.2 RMS
Error from Torque Ripple	0.08 arcsec RMS

The bandwidth frequency is the upper frequency limit on the unit response of the control position to the commanded position. In this case it corresponds to the first eigenvalue of the closed loop system.

5.1.2 Non-Linear Results: Several runs were made to check errors resulting from sources of non-linearity, such as motor saturation and the encoder resolution. These were found not to be an issue, as long as the encoder resolution is at least 0.33 arcsec.

5.2 Elevation Results:

5.2.1 Linear Results: The elevation cases that were modeled are shown in the table below. The disturbance values for each model simulation are the same so that the dynamics can be compared directly. Though the elevation inertia is not a function of elevation angle, the gear ratio is, since the effective moment arm of the linear actuator changes with elevation angle yielding different dynamics at different angles. The moment arm is greatest between 30° and 45°, resulting in a larger gear ratio. Measurements in the literature show that the torque due to wind is likely to be highest when the angle between the dish and the wind is around 30°-45°.

TABLE 5 Modeled Elevation Cases

NAME	INERTIA kgm^2	GEAR RATIO	ELEVATION ANGLE
1. CFRP/CFRP	12236	3490:1	30°
2. Steel/CFRP/Alum	19103	5338:1	30°
3. CFRP/CFRP	12236	2920:1	Zenith
4. CFRP/CFRP-Reduced Imbalance	14580	2090:1	30°

In all the cases the motor inertia was $8.2e^{-4}$ kgm^2, the inertia of the Moog model 304-151A brushless torquer. The next table shows the results of the various model simulations.

TABLE 6 Elevation Simulation Results

1. PARAMETERS- CFRP/CFRP-30°	
Lowest Closest Loop Frequency	4
Step Response-- Overshoot	<10%
Step Response-- Settling Time	2 sec
Tracking Error in 14 m/s Wind	0.73 arcsec RMS
Tracking Error from Friction	nominal
Error from Torque Ripple	0.3 arcsec RMS
2. PARAMETERS- Steel/CFRP/Alum.	
Lowest Closest Loop Frequency	2.5
Step Response-- Overshoot	<10%
Step Response-- Settling Time	2 sec
Tracking Error in 14 m/s Wind	1.1 arcsec RMS
Tracking Error from Friction	nominal
Error from Torque Ripple	0.63 arcsec RMS
3. PARAMETERS- CFRP/CFRP-Zenith	
Lowest Closest Loop Frequency	5
Step Response-- Overshoot	<10%
Step Response-- Settling Time	2 sec
Tracking Error in 14 m/s Wind	0.96 arcsec RMS
Tracking Error from Friction	nominal
Error from Torque Ripple	N/A
4. PARAMETERS- CFRP/CFRP-Reduced Imbalance	
Lowest Closest Loop Frequency	18.2 Hz
Step Response-- Overshoot	<10%
Step Response-- Settling Time	1 sec
Tracking Error in 14 m/s Wind	0.59 arcsec RMS
Tracking Error from Friction	nominal
Error from Torque Ripple	0.2 arcsec RMS

The dish position response to command signal bandwidth is very low in the first three cases. This seems to be the result of the tachometer feedback on the motor put there to maintain a stable control loop. Though tachometer feedback is required in all case where a motor is driving an inertia through a compliant drive, a large amount was necessary here to deal with the large reflected motor inertia. The net result is that the system begins to loss fidelity of response to position commands that are faster than 4-5 Hz. For the most part this is not a problem since this frequency range encompasses most of the disturbances that were modeled.

5.2.2 Non-linear Results: A non-linear model was run twice to test the effect of the encoder resolution. These runs can not be compared directly to the linear runs because real wind data was used in the linear case and calculated wind was used in the non-linear case. The runs showed that with a resolution of 0.33 arcsec, the encoder would not dominate the response.

	A	B	C	D	E	F	G	H	I	J	K
1	**TAM20**	Surface	Pointing	Focus	Phase	BUS max ABS	BFP residuals		REACTIONS		
2	25-Sep-91	rms	error	error	error	displacemen	min	max	Fy	Fz	Mx
3		(μm)	arc sec	(μm)	(μm)	(mm)	(μm)	(μm)	(N)	(N)	(mN)
4	Gravity Zenith	4.3	-0.1	339	31	0.209	-6.2	8.5	0	41725	64
5	Gravity Horizon	6.7	-10.6	3	0	1.226	-16.3	16.3	-41725	0	-9618
6	Wind El=0 front	0.6	-0.5	66	10	0.040	-1.6	1.5	-88	3533	366
7	Wind el=30	0.5	-1.9	57	8	0.042	-0.8	0.9	-8	3169	303
8	Wind el=50	1.5	-1.7	53	7	0.072	-2.8	4.3	218	3019	-655
9	Wind El=70	1.2	-0.2	24	4	0.080	-2.5	3.1	370	1421	-1373
10	Wind El=90	1.4	-1.0	16	3	0.106	-3.1	3.1	492	659	-1727
11	Th1 20C all, incl ring	3.1	0.8	180	101		-5.8	3.9			
12	Th2 2C ring+hub	2.9	0.1	-57	-5		-9.4	2.6			
13	Th3 2C M1	1.0	0.0	101	16		-1.4	1.0			
14	Th4 2C y-lin grad	0.0	0.7	0	0		-0.1	0.1			
15	Th5 2C z-lin grad	0.6	0.1	54	5		-0.5	2.4			
16	Th6 2C M2+Quad	0.7	0.0	14	20		-2.3	2.6			
17	Th7 2C in Ring	0.6	0.0	4	1		-1.6	1.1			

App. 18

8. REFERENCES:

1. *Results of Wind Spectrum Literature Search* DATE: July 9, 1990
2. *Measurement of Wind at Mauna Kea Site* DATE: August 22, 1990
3. *Preparation of the Wind Monitor* DATE: April 24, 1991
4. *MMT Feasibility of Rolling-Element Azimuth Bearings for the MMT Mount* DATE: October 16, 1972
5. *Rotek Wire-Race Bearings Engineering Report* DATE: 1976